GEOFIZIKA VOL. 42 2025

DOI: https://doi.org/10.15233/gfz.2025.42.1
Original scientific paper

Human thermal load on foggy and cloudless mornings in the cold season

Ferenc Ács[1], *Erzsébet Kristóf*[1] *and Annamária Zsákai*[2]

[1] Department of Meteorology, Faculty of Science, Institute of Geography and Earth Sciences, Eötvös Loránd University, Budapest, Hungary

[2] Department of Human Anthropology, Faculty of Science, Eötvös Loránd University, Budapest, Hungary

Received 24 June 2024, in final form 19 December 2024

We investigated the human thermal load in Martonvásár (Hungarian lowland, Carpathian region) in anticyclonic weather conditions in the morning, when a) the sky was completely clear and on the other hand, when b) there was fog. A customizable clothing thermal resistance-operative temperature model was used. The body mass index and the basal metabolic flux density values of the person in the simulations were 25 kg m^{-2} and 40 W m^{-2}, respectively. During the observations, weather data was provided by the automatic station of the HungaroMet company and it was accessible on the company's website. We had 77 observations in foggy weather, while we had 46 observations under clear-sky conditions in the period 2019–2023. The following main results should be highlighted: 1) clothing thermal resistance (r_{cl}) varied between 0.5–2.5 clo in the case of fog, while in clear-sky cases r_{cl} was between 0.9–3.5 clo. 2) Based on our data analysis, we estimated that the warming effect of the morning fog was around 0.8 clo. 3) We also showed that the effect of inter-personal variability on r_{cl} was significant when the heat deficit was high ($r_{cl} \geq 2.5$ clo) and at this time it was comparable with the degree of the warming effect of fog. It should be mentioned that the analysis of typical weather situations from the point of view of human thermal load is a new field of research, since there is little information available on this subject.

Keywords: human thermal load, foggy mornings and clear-sky mornings, Hungarian lowland, thermal resistance of clothing, operative temperature, human data

1. Introduction

The weather in and of itself can be analyzed without taking living beings in regard, that is, objectively, to better understand and discover how the atmosphere works (Radinović, 1968). On the other hand, weather can also be analyzed

in terms of its effects on living beings. Planet Earth is living the age of human dominance (Mészáros, 2001), our approach is human-centric in everything (Rovelli, 2019), so we are mostly interested in finding out how weather affects people's lives (Lim, 2020). This impact can be approached in a broader sense, for instance, by thinking of industries such as tourism (Kovács, 2014), health (Motlogeloa and Fitchett, 2023), recreation (Schiller, 2001), but it can also be narrowed down, directly to the lives of people (Blazejczyk and Krawczyk, 1994). The thermal load of weather has a direct and obvious effect and determines people's daily lives. The thermal load of the weather can only be fully characterized by analyzing the energy balance of the human body (Blazejczyk and Krawczyk, 1994). Energy balance-based methods have mostly been used in two types of studies: human comfort studies (Gulyás et al., 2006; Kántor et al., 2012) and studies dealing with weather situations of extreme thermal load (Bašarin et al., 2018). Extreme thermal load can be extreme heat excess (Bašarin et al., 2020) and/or extreme heat deficit (Auliciems and de Freitas, 1976). Former studies have become more widespread than the latter ones since it was discovered that extreme heat loads could be correlated with deaths (Nastos and Matzarakis, 2012) and illnesses (Motlogeloa and Fitchett, 2023; Yard et al., 2010). The study of human reactions induced by heat stress (*e.g.* thermal perception, sweating) is less widespread, as this would involve examining many people due to the high individual variability. Measuring and observing reactions requires a careful procedure even in the case of one person (Ács et al., 2023, Ács et al., 2024). To avoid having to investigate a lot of people, the concept of "reference human" is used in human biometeorological modeling.

In this study, we focus on weather situations that cause a lack of heat. This is during anticyclonic weather conditions in continental areas in the autumn and winter mornings. This is when the continental areas are the coldest. Mornings can be foggy, cloudy and completely cloudless with clear skies. We will focus on foggy and cloudless conditions and compare them as well. These thermal loads are estimated not for one, but for three different persons, so we can compare the effect of individual human variability with the effect caused by weather differences. To the best of our knowledge, no one has yet conducted such an investigation.

The aim of this study is to estimate the human thermal load 1) under clear-sky conditions and 2) in fog during autumn and winter mornings, 3) to analyze the effect of the radiation characteristics of the environment on human thermal load by comparing foggy and clear-sky situations, as well as 4) to test the sensitivity of human thermal load to interpersonal variability among people. The model we used in our study is a clothing thermal resistance (r_{cl})–operative temperature (T_o) model. The r_{cl}–T_o model was chosen due to its simplicity and because it is suitable for investigating the effect of human interpersonal variability on human thermal load. The observations were carried out in the lowland region of the Carpathian Basin.

2. Materials and methods

In the following, we will talk about the model, the parameterizations used, and we will provide basic information about documenting morning weather situations (fog or clear sky).

2.1. The clothing thermal resistance-operative temperature model

The basic equations of the model are the equations of the thermal resistance of clothing and the operative temperature. They are as follows,

$$r_{cl} = \rho \cdot c_p \cdot \frac{T_S - T_o}{M - \lambda E_{sd} - \lambda E_r - H_r - W} - r_{Hr}, \tag{1}$$

$$T_o = T_a + \frac{R_{ni}}{\rho \times c_p} \times r_{Hr}, \tag{2}$$

where ρ is air density [kgm^{-3}], c_p is specific heat at constant pressure [J kg^{-1} °C^{-1}], T_S is skin temperature (34 °C) (Campbell and Norman, 1997), To is the operative temperature [°C], r_{Hr} is combined resistance for expressing thermal radiative and convective heat exchange effect [s m^{-1}], M is metabolic heat flux density [W m^{-2}], it refers to a person walking at a speed of 1.1 m s^{-1}. λE_{sd} is latent heat flux density of dry skin [W m^{-2}], λE_r is respiratory latent heat flux density [W m^{-2}], H_r is respiratory sensible heat flux density [W m^{-2}], and W is mechanical work flux density [W m^{-2}], T_a is air temperature at a height of 2 m [°C] and R_{ni} is isothermal net radiation [Wm^{-2}]. It should be mentioned that r_{cl} is usually expressed in units of [clo], 1 [clo] = 0.155 m^2 K W^{-1}. If $r_{cl}/(\rho \cdot c_p)$ = 1 [clo], then r_{cl} = 1.2 [kg m^{-3}]×1004 [J kg^{-1} K^{-1}] · 0.155 [m^2 K W^{-1}] = 186.74 [s m^{-1}]. We can see that in this study we took the air density to be 1.2 kg m^{-3}. This can obviously vary with the altitude of the location. Both parameters characterize the thermal load of the air, the former through the thermal insulation of clothing, while the latter through an integrated temperature (dimension °C) value. The derivation of the equations is presented in Appendix A. The parameterizations of R_{ni}, r_{Hr}, M, λE_{sd}, λE_r, H_r and W are presented in Appendix B.

2.2. Documenting atmospheric conditions on foggy and clear-sky mornings

Observations were made between 2017 and 2023. Data collection was carried out in the autumn and winter months: September, October, November, December, January, and February. The morning period is from 6 to 10 a.m. for fog, and from 5 to 8 a.m. for clear skies, with one clear-sky observation between 1 and 2 a.m. In both cases, most of the observations took place between 6 and 8 a.m. The atmospheric conditions are characterized by the following meteorological elements: air temperature, relative sunshine duration, cloud cover, wind gust speed, average wind speed, relative humidity, and air pressure. The values of the me-

teorological elements are average values for a 10-minute period. Global radiation values expressed in W m^{-2} are also 10-minute values. These were determined using the formula (A8) in Appendix B based on the observation of the relative sunshine duration for a 10-minute period. The values of the Q_0 and α constants (see Tabs. B1 and B2 in Appendix B) were obviously taken for the hour in which the 10-minute period occurred.

2.3. Location

The region and the location of the observations can be seen in Fig. 1.

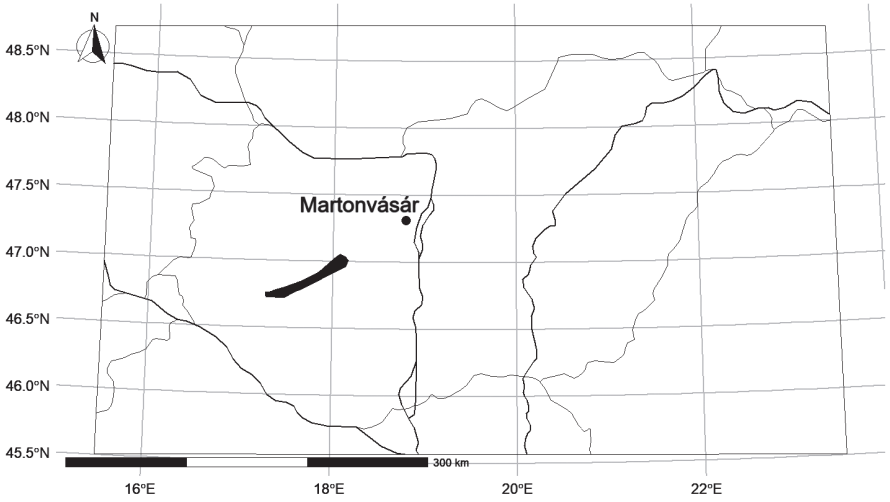

Figure 1. Map of Hungary and Martonvásár (47.31° N, 18.79° E), the location of weather observations during foggy and clear-sky mornings.

Martonvásár is a small lowland town in the Central Transdanubian region of Hungary, about 30 km southwest of Budapest, Hungary. According to Feddema (Ács et al., 2015), the climate of Martonvásár is "cool, dry, with extreme temperature fluctuations", the annual clothing thermal resistance value is around 0.4–1.0 clo (Ács et al., 2020, 2021). However, the weather can cause a much greater lack of heat in the winter season, when the thermal resistance values of clothing can be higher than 3 clo (Ács et al., 2023).

3. Data

We used anthropometric and weather data, briefly described below.

3.1. Anthropometric data

There is a Hungarian anthropometric database (Utczás et al., 2015; Zsákai and Bodzsár, 2016; Fehér et al., 2019) with the anthropometric data of more than

Table 1. Anthropometric data and M_b values of the 3 selected persons.

Person	Sex	Age [Years]	Body mass [kg]	Body length [cm]	Basal metabolic heat flux density [W m^{-2}]	Body mass index [kg m^{-2}]
person 1	male	68	89	190	39.56	24.65
person 2	male	53	95	179	41.81	29.65
person 3	male	24	120	179	45.93	37.45

2,000 children and more than 1,000 adults. The dataset is a product of the Department of Biological Anthropology, Eötvös Loránd University, Budapest, Hungary. We also calculated M_b and body mass index (*BMI*) (for definition, see Appendix C) values from the measured and queried data. From the database, we selected the data of three people among whom the individual deviation is quite large, these data (body mass, body length, sex and age) together with the M_b values are illustrated in Tab. 1.

We chose the persons to maximize the representation of individual variability. It should be mentioned that the weather observations were made by person 1.

3.2. Weather data

When the Carpathian region is dominated by an anticyclone, two opposite weather situations can develop: 1) cloudless weather with a clear sky and 2) weather characterized by fog. We collected data on these two weather types in autumn and winter mornings, when the environmental heat deficit is greatest. The meteorological elements for characterizing thermal load of weather – *i.e.*, air temperature, relative sunshine duration, cloud cover, wind gust speed, average wind speed, relative humidity of air and air pressure – were taken from the HungaroMet website (https://www.met.hu/en/idojaras/aktualis_idojaras/megfigyeles/) and transcribed into the database. The station's instruments consist of sensors belonging to the Vaisala-QLC50 type automatic measurement system. Temperature and humidity are measured by HMP 35D and HMP 35A temperature and humidity probes. Temperature and relative humidity can be read with an accuracy of 0.2 °C and 1%. The beeline distance between the station and the observer's location (garden of a family house) is shorter than 3 km. Relative sunshine duration and cloudiness were observed. Cloudiness and relative sunshine duration are estimated visually in tenths. Their values refer to the same 10 min period as the HungaroMet data. As already mentioned, the values of the radiation parameters (Q_0 and a, Tabs. B1 and B2 in the Appendix B) should be selected for the hour in which the 10-minute observation took place. The input data are available in Tabs. S1 and S2 of the Supplementary Material separately for clear skies and fog, respectively. A total of 122 observations were made (77 in the case of fog and 45 in the case of clear skies). Our regular observations lasted from October 26, 2019 to February 21, 2023, and we also have two observations from 2017. The most important features of the two weather types are presented below.

3.2.1. Weather on foggy mornings

The air temperature varied between –5.5 and 12.0 °C, but in the vast majority of cases it occurred between –2 and 6 °C. The global radiation was very low, it was never higher than 110 W m^{-2}, and in most cases, it was lower than 50 W m^{-2}. By definition, cloud cover is 1, but in three cases we registered rising fog, at which time we estimated cloud cover values of 0.8, 0.5 and 0.4. The relative humidity of the air is by definition 100% or very close to 100%. In fog, wind speeds are usually lower (below 1.5 m s^{-1}), but values higher than 2.5 m s^{-1} can occur. Air pressure was less than 1013 hPa in 10% of the cases (8 cases in total).

3.2.2. Weather on cloudless mornings

The air temperature varied between –12.7 and 13.3 °C. 65% of the temperature values are less than 0 °C. The global radiation varied between 0 and 250 W m^{-2}, with only two values exceeding 200 W m^{-2}. The global radiation was equal to 0 in 15 cases (33%). Cloud cover varied between 0 and 0.2 with values of 0.2 in three cases and 0.1 in two. The relative humidity ranged between 72 and 100% with values exceeding 90% in 69% of the cases (31 cases in total). In most cases, the wind speed was low (less than 1.5 m s^{-1}). Only once (on February 21, 2023 at 8:30 a.m.) was there a stormy wind (gust speed 12.2 m s^{-1}, average wind speed 7.8 m s^{-1}), although the weather was not anticyclonic.

4. Results

We will examine the thermal load of foggy and clear-sky mornings by analyzing the r_{cl} and r_{cl}–T_0 relationship. We will separately analyze a) the thermal load of foggy and b) clear-sky mornings, c) the sensitivity of r_{cl} to the radiation characteristics of the environment comparing foggy and clear-sky situations, d) the sensitivity of thermal loads to human variability and e) the sensitivity of thermal load to the parameterization of clear-sky emissivity. Before discussing these subsections, we will also discuss the human variability by analyzing the individual M_b–*BMI* relationships.

4.1. The M_b–BMI relationship

The M_b – *BMI* value pair is unique for each person making it useful to examine human variability. Fig. 2. shows the M_b–*BMI* relationships for men and women based on the use of data from the Hungarian anthropometric database.

The M_b–*BMI* points of the 3 selected persons are marked in black in Fig. 2. Small *BMI* values (values around 15 kg m^{-2}) are represented by children. In the range of $BMI \leq 25$ kg m^{-2}, 75% of the points refer to children and 25% to adults. These results show that the 3 selected adults differ significantly, despite their M_b values differing by less than 7 W m^{-2}. However, it is worth noting that the difference of 7 W m^{-2} means a relative difference of 18%.

Figure 2. Point cloud representing the dependence of the basal metabolic heat flux density of men (black) and women (gray) on body mass index (*BMI*). The points of persons 1 (circle), 2 (square), and 3 (triangle) (Tab. 1) are marked in black. Sources of the data: Utczás et al. (2015), Zsákai and Bodzsár (2016), and Fehér et al. (2019). Fig. 2 is the same as Fig. 4 in Kristóf et al. (2024).

4.2. Thermal load of foggy and clear-sky mornings

The $r_{cl} - T_0$ relationship for foggy and clear-sky mornings can be seen in Fig. 3.

Foggy cases are marked with black triangle, while clear-sky cases are marked with gray circles. In foggy situations, r_{cl} varied between 0.5 and 2.5 clo, but in

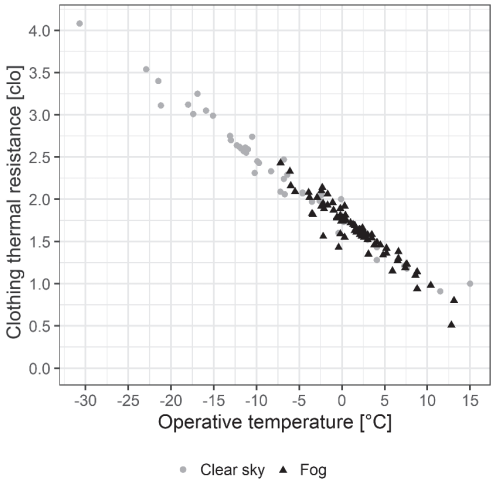

Figure 3. Scatter chart of the clothing thermal resistance of person 1 walking at a speed of 1.1 m s^{-1} as a function of operative temperature on foggy and clear-sky mornings.

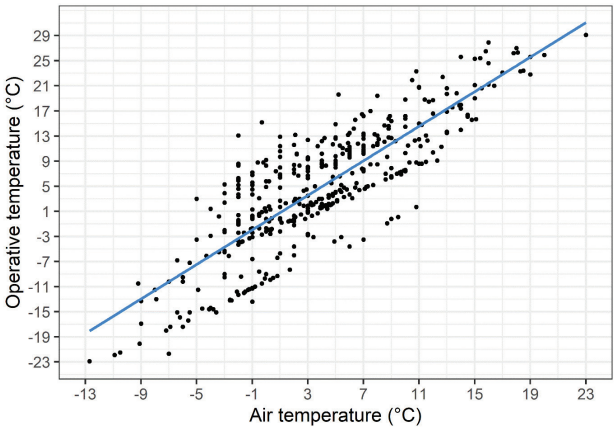

Figure 4. Scatter chart of the operative temperature as a function of air temperature in heat deficit situations.

most cases the values were between 1.25 and 2.0 clo. These values refer to the observer (person 1) who is walking at a speed of 1.1 m s^{-1}. Note that in only three cases were the r_{cl} values smaller than 1 clo.

In clear-sky cases, the r_{cl} values varied between 0.9 and 3.5 clo. We had only 2 cases, when r_{cl} was equal to or less than 1 clo. We can see that most of the r_{cl} values are greater than 1.9 clo. We also have a point with a value of 4.1 clo (the associated T_0 value is –30.7 °C), which refer to the Bükk Mountains. We will refer to this point later in Section 5.

The r_{cl}–T_0 relationship can be better interpreted on the basis of a scatter chart that illustrates the T_0–T_a relationship. Such a point cloud is shown in Fig. 4 in cases of heat deficiency.

The observations were made during the cold season of the period 2018–2022. The cloud cover varied between 0 and 1, and there are about 400 observation points. As can be seen, the range of T_0 is larger than the T_0 range shown in Fig. 3, it is between –23 and +29 °C. It can be seen that the scatter of the points is larger than for the r_{cl}–T_0 link. The relationship can be described by a straight line. We obtained the following regression line equation: $T_0 = 1.38 \times T_a - 0.59$, $r^2 = 0.71$. More about this subject can be read in the work of Ács et al. (2023).

4.3. Comparison of r_{cl} values on foggy and clear-sky mornings

Obviously, the comparison can only be made for the overlapping range of the r_{cl} values. But first, let's compare the weather for foggy and clear-sky mornings! The following features are similar in the weather between foggy and clear-sky mornings: 1) low temperatures that vary within wide ranges, 2) weak air movement, and 3) near-zero, low insolation. The biggest differences are in cloudiness

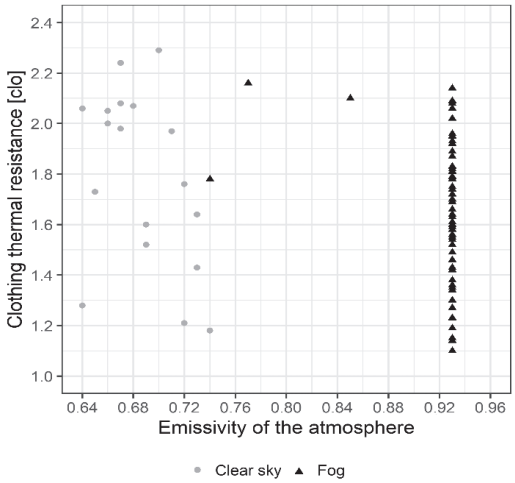

Figure 5. Scatter chart of the clothing thermal resistance of person 1 walking at a speed of 1.1 m s^{-1} as a function of atmospheric emissivity on foggy and clear-sky mornings.

and air humidity. On clear-sky mornings, the humidity is also high, but usually somewhat lower than in the case of foggy mornings. Cloudiness and air humidity have a great effect on the emissivity of the atmosphere, thereby affecting the downward atmospheric radiation (R_{da}) (term 2 in Eq. (A7), APPENDIX B) and thus the surface long-wave radiation of the human body (R_b) (term 3 in Eq. (A7), APPENDIX B). Therefore, the r_{cl}–ε, r_{cl}–R_{da}, and $r_{cl} - R_b$ relationship will be analyzed separately by comparing the cases of foggy and clear-sky mornings.

The point cloud-characterizing the r_{cl}–ε relationship can be seen in Fig. 5.

The ε values are naturally higher (0.92) in the case of foggy mornings (ε_f) than in the case of mornings with a clear sky (0.64–0.74) (ε_{cs}). In both cases, the variability of r_{cl} is determined by the variability of air temperature and air humidity. Because the variability of air humidity is much greater on clear-sky than foggy mornings, the scattering of ${r_{cl}}^{cs}$ values is much greater than the scattering of ${r_{cl}}^{f}$ values. In the case of rising fog (3 points), the ε values are much smaller than in the case of non-rising fog. In this case, the variability of ε values is caused by the variability of cloud cover.

The point cloud characterizing the r_{cl}–R_{da} relationship can be seen in Fig. 6.

${R_{da}}^{f}$ values are higher than ${R_{da}}^{cs}$ values, the difference is usually 60–80 W m^{-2}. According to Fig. 6. ${R_{da}}^{cs}$ values are much more scattered than the ${R_{da}}^{f}$ values. The wide spread of ${R_{da}}^{cs}$ values is caused by the variability of both ε_{cs} and air temperature. Against the former case, the scatter of the ${R_{da}}^{f}$ values is caused only by the variability of the air temperature. We can also see that the ${R_{da}}^{f}$ values of the 3 cases of the rising fog are practically in the point cloud of the ${R_{da}}^{cs}$ values.

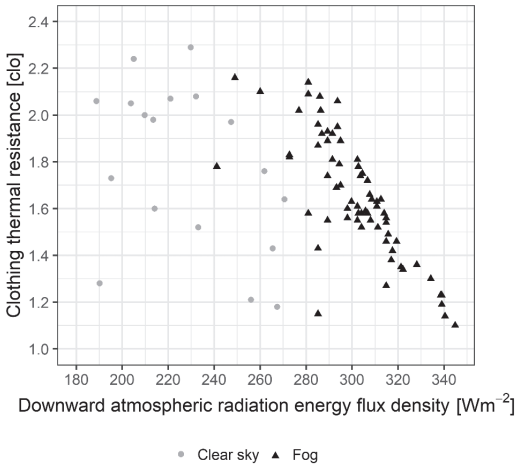

Figure 6. Scatter chart of the clothing thermal resistance of person 1 walking at a speed of 1.1 m s^{-1} as a function of downward atmospheric radiation on foggy and clear-sky mornings.

The point clouds characterizing the r_{cl}-R_b relationship can be seen in Fig. 7.

This figure is similar to Fig. 5, that is, the separation of the foggy, rising fog and clear-sky cases is clearly noticeable. The long-wave radiation balance flux density is negative because the emissivity value of the human body (which is 1) is greater than the emissivity values of the atmosphere. Since $\varepsilon_f > \varepsilon_{rf} > \varepsilon_{cs}$ (where rf stands for rising fog), then $R_b^f > R_b^{rf} > R_b^{cs}$. In foggy cases, the scattering of the r_{cl}^f values is determined only by the variability of the air temperature values. In the 3 cases when there is rising fog, the scattering of the r_{cl}^{rf} values depends on both air temperatures and cloudiness. In the case of mornings with clear skies, the scattering of r_{cl}^{cs} values is caused by the variability of air temperature and air humidity. Important information is that the $R_b^f - R_b^{cs}$ difference is around 80 W m^{-2} regardless of the air temperature. Based on this fact, the combined effect of the heating effect of the fog and the cooling effect of the clear-sky can be estimated.

This effect can be estimated using equation (2) and based on Fig. 3. Let's calculate the magnitude of the $T_o^f - T_o^{cs}$ difference in the cases of a foggy and clear-sky mornings if there is no difference between their values of insolation (there is only long-wave radiation balance), wind speed (which is low) and air temperature (any value between 12 and –6 °C), that is, only cloudiness and air humidity differ between the two cases! Under these conditions, the $T_0^f - T_0^{cs}$ difference can be estimated with the expression [80 / (1.2×1004)]×120, where $\Delta R_{ni} = \Delta R_b = R_b^f - R_b^{cs} = 80$ W m^{-2}, $\rho = 1.2$ kg m^{-3}, $c_p = 1004$ J kg^{-1} °C^{-1} and $r_{Hr} = 120$ s m^{-1} because the wind is weak. The $T_0^f - T_0^{cs}$ difference is 8 °C and if we apply the same human conditions (person 1, walking speed of 1.1 m s^{-1}), we can read the r_{cl} difference belonging to the $T_0^f - T_0^{cs}$ difference from Fig. 3. The resulting difference is the thermal load difference between the fog and the clear sky, which is about 0.8 clo.

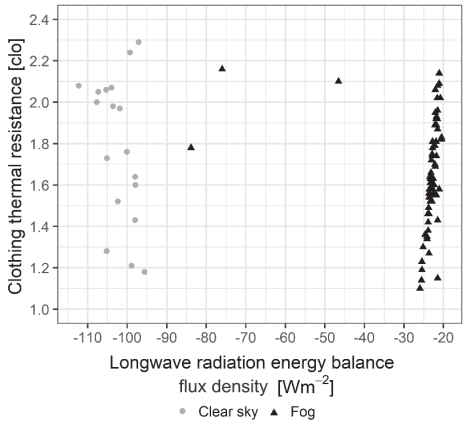

Figure 7. Scatter chart of the clothing thermal resistance of person 1 walking at a speed of 1.1 m s^{-1} as a function of long-wave radiation balance of the human body on foggy and clear-sky mornings.

4.4. Sensitivity of the r_{cl}–T_0 relationship to human interpersonal variability

It is interesting to test the sensitivity of r_{cl}–T_0 relationship to interpersonal variability of M. We executed this separately for cloudless and foggy mornings, comparing person 1 with persons 2 and 3. These point clouds can be seen in Fig. 8 in the cloudless case, while in Fig. 9 in the foggy case.

It is noticeable that as the lack of heat increases, the r_{cl} differences between people also increase. Therefore, the effect of interpersonal variability on r_{cl} values is stronger, even significantly, on cloudless mornings compared to foggy

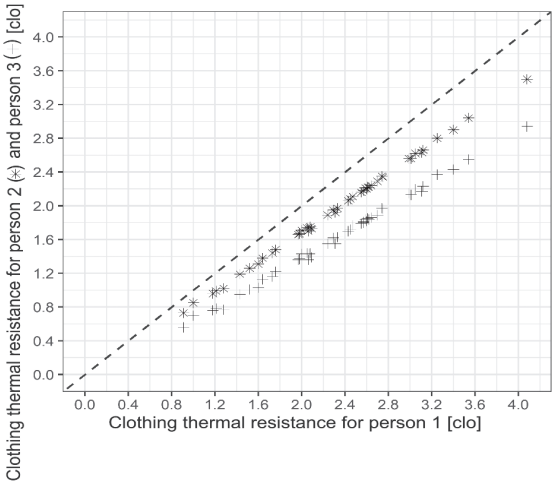

Figure 8. Comparison of clothing thermal resistance values referring to persons 2 and 1 (star) and persons 3 and 1 (cross) on clear-sky mornings. Their walking speed is 1.1 m s^{-1}.

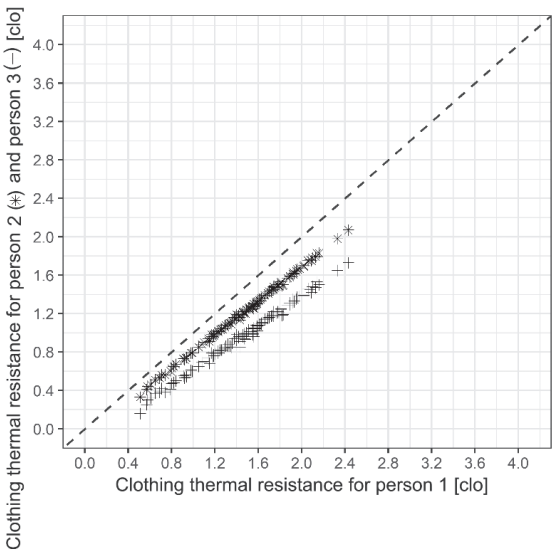

Figure 9. Comparison of clothing thermal resistance values referring to persons 2 and 1 (star) and persons 3 and 1 (cross) on foggy mornings. Their walking speed is 1.1 m s^{-1}.

mornings. How big is this effect on the people being tested? In Fig. 8 (cloudless case), the biggest difference is between people 1 and 3, its value is around 1–1.2 clo (the cross symbol representing the biggest heat deficit), which is around 30% of the actual thermal load. At the same extreme point (comparison of persons 1 and 3 for the highest heat deficit) in Fig. 9 (foggy case), the r_{cl} difference is 0.7–0.8 clo, that is, it is around 50% less than in the clear-sky case. It should also be mentioned that the investigated personal r_{cl} difference in the largest heat deficit (Fig. 8, cross symbol with the largest heat deficit) has a value of 1–1.2 clo and it is comparable to the thermal load difference between foggy and clear-sky weather situations, which we estimated to be around 0.8 clo. The smallest r_{cl} differences are between people 1 and 2 (stars), when the heat deficit is the smallest (values around 0.8–1 clo). Its value is 0.1–0.3 clo, which is around 20% of the thermal load. So, we can see that the interpersonal r_{cl} differences amount to 10–30% of the actual heat deficits.

4.5. Sensitivity of r_{cl} to ε_{cs} parameterizations

The lack of heat in the mornings is mostly determined by cloudiness. In the case of a cloudless sky, the lack of heat is mostly determined by the temperature and humidity of the air, since downward atmospheric radiation strongly depends on these atmospheric state variables. The emissivity of the clear-sky also depends on these state variables, so, it can be parameterized only as a function of air humidity (*e.g.* Brunt's (1932) formula, equation (A9) in Appendix B) or as a func-

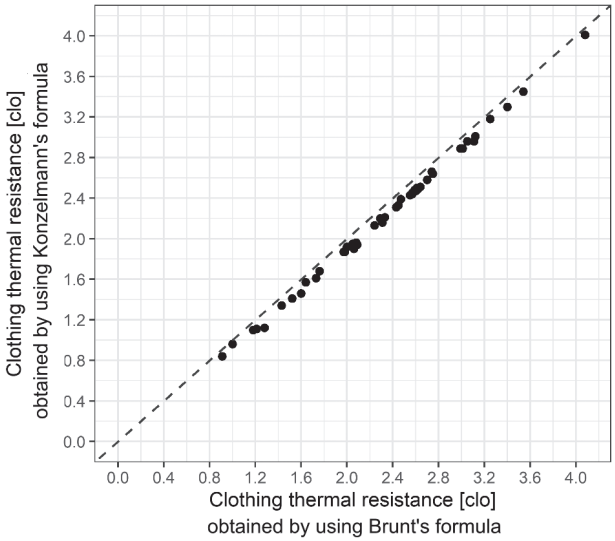

Figure 10. Comparison of clothing thermal resistance values obtained based on ε_{cs} values estimated by the parameterization of Brunt (1932) and Konzelmann (1994) in the case of clear skies. Anthropometric data refer to person 1 walking at a speed of 1.1 m s^{-1}.

tion of air humidity and temperature (*e.g.* Konzelmann's (1994) formula, equation (A10) in Appendix B). It should be noted here that none of the formulae consider the effect of air temperature inversion on the ε_{cs} (Cheng et al., 2020). The question arises: how sensitive is r_{cl} to the parameterization of ε_{cs}, naturally, in the case of a cloudless sky? Figure 10 illustrates the sensitivity.

The results refer to person 1 walking at a speed of 1.1 m s^{-1}. The differrences between the obtained r_{cl} values are very small, below 0.2 clo, and the r_{cl} values obtained with formula (A9) (Brunt, 1932) overestimate, albeit minimally, the r_{cl} values obtained with formula (A10) (Konzelmann, 1994).

5. Discussions

Human biometeorology deals with the effects of climate and/or weather on humans. In the center is the person who is either in a state of comfort or discomfort in the given atmospheric environment. The focus is not on the weather itself, but on a person's sense of comfort (Honjo, 2009; Milošević et al., 2016) or discomfort (Blazejczyk et al., 2012; Nastos and Matzarakis, 2012), which is caused by the thermal effect of weather. This issue is rarely discussed in relation to typical (Kristóf et al., 2024) or selected weather situations. Some studies focus on reactions caused by thermal load, such as thermal sensation (Krüger et al., 2021; Ács et al., 2023) or sweating (Havenith et al., 2013).

Human thermal load depends on both environmental and human factors and must be calculated from the energy balance of the human body (Katić et al.,

2016). The calculation requires both human (at least 4 types of data: body mass, body length, sex and age) and meteorological (at least 4 types of data: radiation, air temperature, air humidity and wind speed) data, so we can say that the calculation is data intensive. Collecting human data is more difficult than meteorological data. Human data does not only mean anthropometric data, but also includes data characterizing clothing and activity. It should be emphasized that the variability of data characterizing clothing and activity is enormous. Thus, the "reference human" was introduced into human biometeorological studies. However, the definition of this "reference human" varies by method (Ács et al., 2023). This reduced the data requirements of the models but made it impossible to examine the sensitivity of thermal load to human variability. However, this is not the case for models based on the use of individual human data (Ács et al., 2021). In many cases, the use of meteorological data was also reduced (Bröde et al., 2012). This may even be justified in special cases (windchill), but it can also lead to large errors in estimating thermal load (Ács et al., 2023a).

The use of all available data is very important when estimating the thermal load of the weather, especially if the weather is extreme in some respect. In the Carpathian region, extreme thermal loads occur in anticyclonic weather situations. Then, the mornings of the cold season can be dominated by two completely different weather types: cloudless, mostly calm, but very cold weather with clear sky, or fog, in which the air movement is also weak, and the air is warmer and more humid than in the former weather type. To the best of our knowledge, no one has yet investigated the thermal load of these two opposite weather types or compared their thermal loads, although they are intriguing. Since, based on our model, we can estimate changes in r_{cl} values due to changes in atmospheric and human factors, we can compare these two effects, such as the warming effect of fog, and r_{cl} changes resulting from human variability. We could see that the shift between the r_{cl} values of cloudless (clear-sky) and foggy morning point clouds is around 1–1.5 clo (Fig. 3), and this is comparable to the largest r_{cl} value deviations caused by human variability (Fig. 8, cross symbols). Similarly, in the case of a cloudless sky, we can compare the deviations of the r_{cl} values obtained by different ε_{cs} parameterizations (Fig. 10) with the deviations of r_{cl} values obtained by using individual anthropometric data (Fig. 8). In this case, the r_{cl} value changes caused by human variability are always larger than the r_{cl} value changes caused by parameterizations. We can say that interpersonal differences cannot be neglected when estimating human thermal load on cloudless mornings.

In our opinion, these human thermal load data can be extended to the entire Great Plain. What are these thermal load values in the mountains of Hungary? In the case of fog, we cannot give an estimate, so we assume that the lack of heat in mountain fog is not greater than in lowland fog. However, we can give an estimate of thermal load for cloudless mornings. The biggest differences are in the air temperature, the differences between the values of solar radiation (around zero or zero), air humidity (close to saturation), and wind speed (close to calm conditions) values are very small and negligible. HungaroMet stations have al-

ready recorded temperatures of around –20 °C in the Bükk Mountains in winter in the morning hours. We selected such a case (February 13, 2021, 6:30 a.m.), at which time the heat deficit was 4.1 clo (Fig. 3). In the sinkholes of Bükk-plateau, temperatures could go down to –30 °C (Dobos et al., 2024), in this case the heat deficit is already around 4.8 clo. These thermal deficit values were experienced by person 1 walking at a speed of 1.1 m s^{-1}. We can state that the greatest heat deficit values in Hungary are around 5 clo. This experience is extremely individual, subjective, as it is shown in the study.

Finally, it should be mentioned that the analysis was performed with a specific model, the r_{cl}–T_0 model. The model is a) very simple, and b) applies to individuals, it does not use the concept of a "standard" person and is therefore able to simulate human variability. The model parameterizes global radiation, which is a variable but important environmental thermal load factor. The formula used is the Ångström-type formula (Ångström, 1924), which estimates global radiation as function of relative sunshine duration on a daily or hourly scale. The global radiation and sunshine duration data are collected at the Rimski Šančevi radiation measuring station (geographical latitude 45.3° N and geographical longitude 19.5° E) in the period 1966–1970. Global radiation was measured with a Moll-Gorczynski pyranometer and recorded with a Kipp potentiometric recorder. The sunshine duration data were provided by a Campbell-Stokes sunshine recorder. We can say that the parameterization used is also a specific element of the model. Furthermore, the model parameterizes the long-wave radiation balance in a very simple way. The isothermal radiation approach was used, and the temperature inversion effect was not taken into account in the parameterization of the emissivity for the clear sky. Based on the work of Cheng et al. (2020), this results a bias between 10 and 20 W m^{-2} when estimating R_{da}. Two factors hinder the wider application of the model: 1) the more difficult interpretation of the clothing thermal insulation values, and 2) the fact that the model cannot be used to simulate situations with excess heat as long as the sweating process is not represented. Representing sweating seems to be a major obstacle, as it cannot be simulated deterministically, but only with statistical-deterministic methods (Fiala, 1998). This is a major disadvantage for the model to be routinely applicable. The model can be used not only for human-based weather analysis, but also for climate classification or for optimizing energy consumption in homes (Szalkai et al., 2024). The model is based on energy balance (the imagined clothing is always dry, because it is hydrophobic and ensures thermal balance), so it can be used to analyze and understand the energetics of people moving outdoors, which can also stimulate the easier implementation of the United Nations' Sustainable Development Goals (SDGs) – especially SDG 3 entitled as "Ensure healthy lives and promote well-being for all at all ages" – or to optimize the energy consumption of urban interiors, which is specifically one of the goals of SDG 11. Developing these usage options is one of the future tasks. We are currently developing the model in such a way that we can also analyze summer situations that cause large excess heat.

6. Conclusions

The main conclusions of the study are as follows: 1) the thermal load of the human body is noticeably different in the hours of foggy and clear-sky mornings. 2) Downward atmospheric radiation plays a decisive role in the development of this difference. 3) With the applied model and data, we quantified the magnitude of this thermal load difference, and based on our estimates, it is around 0.8 clo. 4) In extreme heat deficit situations ($r_{cl} \geq 2.5$ clo), the effect of interpersonal variability on r_{cl} is comparable with the difference in thermal load for foggy and clear-sky conditions. 5) In the given environmental heat deficit, it may also happen that the r_{cl} change caused by interpersonal variability is greater than the r_{cl} change caused by the variability of the physical parameter (in our case clear-sky emissivity).

Author contributions: Conceptualization: F. Á.; methodology: F. Á., A. Z.; software: F. Á and E. K.; validation: F. Á.; formal analysis: F. Á., E. K., A. Z.; investigation: F. Á.; resources: F. Á, A. Z.; data curation: F. Á. and A. Z.; writing–original draft preparation: F. Á.; writing–review and editing: F. Á.; visualization: E. K.; supervision: F. Á.; project administration: A. Z. All authors have read and agreed to the published version of the manuscript.

Funding: This research received no external funding.

Conflicts of interest: The authors declare no conflict of interest.

References

Ångström, A. (1924): Solar and terrestrial radiation, *Quart. J. Roy. Met. Soc.*, **50**, 121–125, http://dx.doi.org/10.1002/qj.49705021008.

Auliciems, A. and de Freitas, C. R. (1976): Cold stress in Canada. A human climatic classification, *Int. J. Biometeorol.,* **20**, 287–294, https://doi.org/10.1007/BF01553585.

Auliciems, A. and Kalma, J. D. (1979): A climatic classification of human thermal stress in Australia, *J. Appl. Meteorol.*, **18**, 616–626, https://doi.org/10.1111/j.1467-8470.1981.tb00373.x.

Ács, F., Breuer, H. and Skarbit, N. (2015): Climate of Hungary in the twentieth century according to Feddema, *Theor. Appl. Climatol.,* **119**, 161–169, https://doi.org/10.1007/s00704-014-1103-5.

Ács, F., Zsákai, A., Kristóf, E., Szabó, A. I. and Breuer, H. (2020): Carpathian Basin climate according to Köppen and a clothing resistance scheme, *Theor. Appl. Climatol.*, **141**, 299–307, https://doi.org/10.1007/s00704-020-03199-z.

Ács, F., Kristóf, E., Zsákai, A., Kelemen, B., Szabó, Z. and Marques Vieira, L. A. (2021): Weather in the Hungarian Lowland from the point of view of humans, *Atmosphere*, **12**, 84, https://doi.org/10.3390/atmos12010084.

Ács, F., Zsákai, A., Kristóf, E., Szabó, A. and Breuer, H. (2021): Human thermal climate of the Carpathian Basin, *Int. J. Climatol.*, **41**, E1846–E1859, https://doi.org/10.1002/joc.6816.

Ács, F., Kristóf, E. and Zsákai, A. (2023): Individual local human thermal climates in the Hungarian lowland: Estimations by a simple clothing resistance-operative temperature model, *Int. J. Climatol.*, **43**, 1273–1292, https://doi.org/10.1002/joc.7910.

Ács, F., Szalkai, Z., Kristóf, E. and Zsákai, A. (2023a): Thermal resistance of clothing in human biometeorological models, *Geogr. Pannonica*, **27(2)**, 83–90, https://doi.org/10.5937/gp27-40554.

Ács, F., Kristóf, E. and Zsákai, A. (2024): Weather dependence of heart rate and skin surface evaporation: an analysis for selected summer weather conditions, *Légkör,* **69(4)**, 231–241 (in Hungarian).

Bašarin, B., Lukić, T., Mesaros, M., Pavić, D., Đorđević, J. and Matzarakis, A. (2018): Spatial and temporal analysis of extreme bioclimate conditions in Vojvodina, Nothern Serbia, *Int. J. Climatol.*, **38(1),** 142–157, https://doi.org/10.1002/joc.5166.

Bašarin, B., Lukić, T. and Matzarakis, A. (2020): Review of biometeorology of heatwaves and warm extremes in Europe, *Atmosphere*, **11**, 1276, https://doi.org/10.3390/atmos11121276.

Blazejczyk, K. and Krawczyk, B. (1994): *Bioclimatic Research of the Human Heat Balance*. Polish Academy of Science, Institute of Geography and Spatial Organization, **28**, 66 pp.

Blazejczyk, K., Epstein, Y., Jendritzky, G., Staiger, H. and Tinz, B. (2012): Comparison of UTCI to selected thermal indices, *Int. J. Biometeorol.*, **56**, 515–535, https://doi.org/10.1007/s00484-011-0453-2.

Bröde, P., Fiala, D., Błażejczyk, K., Holmér, I., Jendritzky, G., Kampmann, B., Tinz, B. and Havenith, G. (2012): Deriving the operational procedure for the Universal Thermal Climate Index (UTCI), *Int. J. Biometeorol.*, **56**, 481–494, https://doi.org/10.1007/s00484-011-0454-1.

Brunt, D. (1932): Notes on radiation in the atmosphere, *Q. J. R. Meteorol. Soc.*, **58**, 389–420, https://doi.org/10.1002/qj.49705824704.

Campbell, G. S. and Norman, J. (1998): *An Introduction to Environmental Biophysics*. 2nd Edition, Springer, New York, NY, USA, 286 pp.

Cheng, J., Liang, S. and Shi, J. (2020): Impact of air temperature inversion on the clear-sky surface downward longwave radiation estimation, *IEEE Trans. Geosci. Remote Sens.*, **58**(7), 4796–4802.

Dobos, A., Kerékgyártó, R. and Dobos, E. (2024): Summary analysis of the 2022–2023 winter season based on the measurements in the Mohos-sinkhole and Vörösmeteor-sinkhole in Bükk plateau, *Légkör*, **69**(1), 33–40, https://doi.org/10.56474/legkor.2024.1.5.

Dubois, D. and Dubois, E. F. (1915): The measurement of the surface area of Man, *Arch. Intern. Med.,* **15**, 868–881, https://doi.org/10.1001/archinte.1915.00070240077005.

Fanger, P. O. (1970): *Thermal comfort*. In: Analysis and applications in environmental engineering. Danish Technical Press, Copenhagen, Denmark, 244 pp.

Fehér, V. P., Annár, D., Zsákai, A. and Bodzsár, É. (2019): The determinants of psychosomatic health complaints in 18–90 year-old women (in Hungarian), *Anthrop. Közl.*, **60**, 65–77, https://doi.org/10.20330/AnthropKozl.2019.60.65.

Fiala, D. (1998): Dynamic simulation of human heat transfer and thermal comfort. *PhD Thesis*, De Monfort University Leicester and Fh Stuttgart – Hochschule für Technik, 293 pp, available at: https://www.researchgate.net/publication/35402573_Dynamic_Simulation_of_Human_Heat_Transfer_and_Thermal_Comfort/link/5633311308ae911fcd4a25fc/download?_tp=eyJjb250ZXh0IjpTInBhZ2UiOiJwdWJsaWNhdGlvbiIsInByZXZpb3VzUGFnZSI6bnVsbH19

Frankenfield, D., Roth-Yousey, L. and Compher, C. (2005): Comparison of predictive equations for resting metabolic rate in healthy nonobese and obese adults: A systematic review, *J. Am. Diet. Assoc.,* **105**, 775–789, https://doi.org/10.1016/j.jada.2005.02.005.

Gulyás, Á., Unger, J. and Matzarakis, A. (2006): Assessment of the microclimatic and thermal comfort conditions in a complex urban environment: Modelling and measurements, *Build. Environ.*, **41**, 1713–1722, https://doi.org/10.1016/j.buildenv.2005.07.001.

Gulyás, M. (2018): Parameterization of the atmospheric downward radiation. *BSc Thesis*, Eötvös Loránd University, 42 pp (in Hungarian).

Havenith, G., Bröde, P., Hartog, E., Kuklane, K., Holmer, I., Rossi, R., Richards, M., Farnworth, B. and Wang, X. (2013): Evaporative cooling: Effective latent heat of evaporation in relation to evaporation distance from the skin, *J. Appl. Physiol.*, **114**, 778–785, https://doi.org/10.1152/japplphysiol.01271.2012.

Honjo, T. (2009): Thermal comfort in outdoor environment, *Glob. Environ. Res.*, **13**, 43–47.

Katić, K., Li, R. and Zeiler, W. (2016): Thermophysiological models and their applications: A review, *Building and Environ.*, **106**, 286–300, https://doi.org/10.1016/j.buildenv.2016.06.031.

Kántor, N., Égerházi, L. and Unger, J. (2012): Subjective estimation of thermal environment in recreational urban spaces – Part 1: Investigations in Szeged, Hungary, *Int. J. Biometeorol.*, **56**, 1089–1101, https://doi.org/10.1007/s00484-012-0523-0.

Konzelmann, T., van de Wal, R. S. W., Greuell, W., Bintanja, R., Henneken, E. A. C. and Abe-Ouchi, A. (1994): Parameterization of global and longwave incoming radiation for the Greenland Ice Sheet, *Global Planet. Change*, **9**, 143–164, https://doi.org/10.1016/0921-8181(94)90013-2.

Kovács, A. (2014): Modification of the Tourism Climatic Index to Central European climatic conditions – Examples, *Időjárás*, **118**(2), 147–166.

Kristóf, E., Ács, F. and Zsákai, A. (2024): On the human thermal load in fog, *Meteorology*, **3**, 83–96, https://doi.org/10.3390/meteorology3010004.

Krüger, E. L., Vieira Silva, T. J., Silveira Hirashima, S. Q., Cunha, E. G. and Rosa, L. A. (2021): Calibrating UTCI'S comfort assessment scale for three Brazilian cities with different climatic conditions, *Int. J. Biometeorol.*, **65**, 1463–1472, https://doi.org/10.1007/s00484-020-01897-x.

Lim, C. L. (2020): Fundamental concepts of human thermoregulation and adaptation to heat: A review in the context of global warming, *Int. J. Environ. Res. Public Health*, **17**, 7795, https://doi.org/10.3390/ijerph17217795.

Mészáros, E. (2001): *A Brief History of Earth. Past, Present. Future.* Vince Publishing, Budapest, 167 pp (in Hungarian).

Mifflin, M. D., St. Jeor, S. T., Hill, L. A., Scott, B. J., Daugherty, S. A. and Koh, Y. O. (1990): A new predictive equation for resting energy expenditure in healthy individuals, *AJCN*, **51**, 241–247, https://doi.org/10.1093/ajcn/51.2.241.

Mihailović, D. T. and Ács, F. (1985): Calculation of the daily amount of global radiation in Novi Sad, *Időjárás*, **89(5)**, 257–261.

Milošević, D., Savić, S., Marković, V., Arsenović, D. and Šećerov, I. (2016): Outdoor human thermal comfort in local climate zones of Novi Sad (Serbia) during heat wave period, *Hung. Geogr. Bull.*, **65**(2), 129–137. https://doi.org/10.15201/hungeobull.65.2.4.

Motlogeloa, O. and Fitchett, J. M. (2023): Climate and human health: A review of publication trends in the International Journal of Biometeorology, *Int. J. Biometeorol.*, **67**, 933–955, https://doi.org/10.1007/s00484-023-02466-8.

Nastos, P. T. and Matzarakis, A. (2012): The effect of air temperature and human thermal indices on mortality in Athens, Greece, *Theor. Appl. Climatol.*, **108**, 591–599, https://doi.org/10.1007/s00704-011-0555-0.

Radinović, D. (1969): *Weather analaysis*. Institute for Publishing Textbooks of the Socialist Republic of Serbia, Belgrade, 367 pp (in Serbian).

Rovelli, C. (2019): *Reality is not what we see it to be*, 2nd Edition, Park Book Publishing, Budapest, 239 pp (in Hungarian).

Schiller, G. (2001): Biometeorology and recreation in east Mediterranean forests, *Landsc. Urban Plan.*, **57**(1), 1–12, https://doi.org/10.1016/S0169-2046(01)00182-7.

Szalkai, Z., Ács, F. and Kristóf, E. (2024): How to optimize the heating and cooling of homes with simple steps?, in: *Current doctoral research at the Department of Meteorology*, edited by: Kiss, A. and Pongrátz, R. ELTE, Department of Meteorology, Budapest, 73–77 (in Hungarian), https://doi.org/10.31852/EMF.36.2024.073.077.

Utczás, K., Zsákai, A., Muzsnai, Á., Fehér, V. P. and Bodzsár, É. (2015): The analysis of bone age estimations performed by radiological and ultrasonic methods in children aged between 7–17 years, *Anthrop. Közl.,* **56**, 129–138 (in Hungarian), https://doi.org/10.20330/AnthropKozl.2015.56.129.

Weyand, P. G ., Smith, B. R., Puyau, M. R. and Butte, N. F. (2010): The mass-specific energy cost of human walking is set by stature, *J. Exp. Biology*, **213**, 3972–3979, https://doi.org/10.1242/jeb.048199.

Zsákai, A. and Bodzsár, É. (2016): The relationship between reproductive ageing and the changes of bone structure in women, *Anthrop. Közl.*, **57**, 77–84 (in Hungarian), https://doi.org/10.20330/AnthropKozl.2016.57.77.

Yard, E. E., Gilchrist, J., Haileyesus, T. and Murphy, M. (2010): Heat illness among high school athletes – U. S., 2005–2009, *J. Safety Res.*, **41(6)**, 471–474, https://doi.org/10.1016/j.jsr.2010.09.001.

SAŽETAK

Ljudsko toplinsko opterećenje u maglovitim i bezoblačnim jutrima u hladnoj sezoni godine

Ferenc Ács, Erzsébet Kristóf i Annamária Zsákai

Istraživali smo toplinsko opterećenje čovjeka u Martonvásáru (Mađarska nizina, Karpatsko područje) u anticiklonalnim vremenskim uvjetima ujutro, kada je a) nebo bilo potpuno vedro, i sa druge strane, kada je b) bilo magle. Koristili smo jedan prilagodljivi model toplinske otpornosti odjeće i operativne temperature. Vrijednosti indeksa tjelesne mase i bazalnog metaboličkog protoka osobe u simulacijama bile su 25 kg m^{-2} odnosno 40 W m^{-2}. Tijekom promatranja podatke o vremenu je merila automatska postaja tvrtke HungaroMet i ti podaci su bili dostupni na web stranicama tvrtke. Imali smo 77 promatranja po maglovitom vremenu, dok smo imali 46 promatranja po vedrom vremenu u razdoblju od 2019. do 2023. godine. Treba istaknuti sljedeće glavne rezultate: 1) toplinska otpornost odjeće (r_{cl}) varirala je između 0,5–2,5 clo u slučaju magle, dok je u slučajevima vedrog neba r_{cl} vrednost bila između 0,9–3,5 clo. 2) Na temelju naše analize podataka, procijenili smo da je učinak zagrijavanja jutarnje magle oko 0,8 clo. 3) Također smo pokazali da je učinak međuljudske varijabilnosti na r_{cl} bio značajan kada je deficit topline bio visok ($r_{cl} \geq 2{,}5$ clo) i u to vrijeme bio je usporediv sa stupnjem učinka zagrijavanja magle. Valja napomenuti da je analiza tipičnih vremenskih situacija sa stajališta ljudskog toplinskog opterećenja novo područje istraživanja, budući da o tome postoji malo podataka.

Ključne riječi: ljudsko toplinsko opterećenje, maglovita jutra i vedra jutra, Mađarska nizina, toplinska otpornost odjeće, operativna temperatura, ljudski podaci

Corresponding author's address: Ferenc Ács, Department of Meteorology, Faculty of Science, Institute of Geography and Earth Sciences, Eötvös Loránd University, Budapest, Hungary; e-mail: acs@staff.elte.hu

APPENDIX A.

Derivation of the basic equations

The equations that calculate r_{cl} and T_0 (Eqs. (1) and (2)) are the basic equations of the model. We can obtain these as follows. The model does not contain a storage term and does not parameterize the phenomenon of sweating. By ignoring these phenomena, the energy balance of clothing and skin surfaces are as follows:

$$R_{ni} + H_S + \lambda E_{sd} - H_{cl} - \lambda E_{cl} = 0, \tag{A1}$$

$$H_S = M - \lambda E_{sd} - \lambda E_r - H_r - W, \tag{A2}$$

where H_S is the sensible heat flux density between skin surface and clothing [W m^{-2}], H_{cl} is the sensible heat flux density between the clothing surface and the near surface atmosphere [W m^{-2}], λE_{sd} is latent heat flux density of dry skin [W m^{-2}], λE_{cl} is the latent heat flux density of the clothing surface [W m^{-2}], M is the metabolic heat flux density of a walking human [W m^{-2}], λE_r is respiratory latent heat flux density [W m^{-2}], H_r is respiratory sensible heat flux density [W m^{-2}], W is the mechanical work flux density of muscles of a walking human [W m^{-2}]. Since there is no storage $\lambda E_{sd} = \lambda E_{cl}$. H_S can be expressed either via body temperature T_b (37 °C) or via clothing temperature T_{cl} as follows:

$$H_S = \rho \times c_p \times \frac{T_b - T_S}{r_t}, \tag{A3}$$

$$H_S = \rho \times c_p \times \frac{T_S - T_{cl}}{r_{cl}}, \tag{A4}$$

where r_t is the tissue resistance [sm^{-1}]. Equating Eqs. (A3) and (A4), we can get T_{cl}. Replacing it into (A1) and using Eqs. (A2) and (A3), we can get the following energy balance equation for clothing:

$$R_{ni} + \left(1 + \frac{r_{cl}}{r_{Hr}}\right) \times (M - \lambda E_{sd} - \lambda E_r - H_r - W) - \rho \times c_p \times \frac{T_S - T_a}{r_{Hr}} = 0 \tag{A5}$$

R_{ni} and T_a are the most important environmental forcings in Eq. (A5). The thermal impact of R_{ni} can be expressed by introducing operative temperature T_0 putting $T_a = T_0$ when $R_{ni} = 0$. Doing so, we can get the following equation:

$$M - \lambda E_{sd} - \lambda E_r - H_r - W = \rho \times c_p \times \frac{T_S - T_o}{r_{Hr} + r_{cl}}, \tag{A6}$$

We can see that Eq. (1) can be easily obtained from eq. (*A*6). Eq. (2) can also be easily obtained replacing Eq. (*A*6) back into Eq. (*A*5). In Eq. (2), T_0 depends only upon environmental variables.

APPENDIX B.

Parameterizations

To use Eqs. (1), (2), R_{ni}, r_{Hr}, M, λE_{sd}, λE_r, H_r, and W need to be parameterised.

Parameterization of R_{ni}

R_{ni} is calculated as simply as possible,

$$R_{ni} = S \times \left(1 - \alpha_{cl}\right) + \varepsilon_a \sigma T_a^4 - \varepsilon_{cl} \sigma T_a^4, \tag{A7}$$

where S is global radiation, α_{cl} is clothing albedo, ε_a is atmospheric emissivity, ε_{cl} is the emissivity of clothing or skin, and σ is the Stefan–Boltzmann constant [5.67 W m^{-2} K^{-4}]. S is estimated by parameterization (Mihailović and Ács, 1985), α_{cl} = 0.25–0.27, ε_{cl} = 1 and ε_a depends on clear-sky emissivity ε_{cs} and cloudiness N (0 for cloudless and 1 for completely overcast conditions). S depends upon relative sunshine duration *rsd* as,

$$S = Q_0 \times \left[\alpha + (1 - \alpha) \times rsd\right] \tag{A8}$$

where Q_0 is the global radiation constant [MJ m^{-2} hour^{-1}] referring to clear-sky conditions and a 1-hour time period and α is the corresponding dimensionless constant referring to the same hour. Eq. (*A*8) is the well-known Ångström-type formula (Ångström, 1924) adapted for lowland conditions in the Carpathian Basin. It should be noted that the hourly values of Q_0 can also be applied to smaller time intervals within the hour, if the relative sunshine duration value for the smaller time interval is known or available. In this study, the shorter time units were always 10 minutes. The hourly values of Q_0 and a are contained in Tabs. B1 and B2.

There are many parameterizations for clear-sky emissivity (Gulyás, 2018). There are parameterizations that depend a) only on air temperature, b) only on water vapor pressure and c) on both air water vapor pressure and temperature. We chose a parametrization from the latter two methods, namely Brunt (1932) (it depends only on partial water vapor pressure), and Konzelmann et al. (1994) (it depends on both partial water vapor pressure and temperature) formulae,

$$\varepsilon_{cs} = 0.51 + 0.066 \times \sqrt{e_a}, \tag{A9}$$

$$\varepsilon_{cs} = 0.23 + 0.4393 \times \left(\frac{e_a}{T_a}\right)^{\frac{1}{7}}, \tag{A10}$$

Table B1. Average hourly values of the Q_0 constant [MJ m^{-2} $hour^{-1}$] during the day in the months of the year. The values were determined from the measured global radiation and sunshine duration time series in Novi Sad in the period 1966–1970.

Start hour	End hour	J	F	M	A	M	J	J	A	S	O	N	D
4	5	0.000	0.000	0.000	0.000	0.523	0.155	0.243	0.000	0.000	0.000	0.000	0.000
5	6	0.000	0.000	0.000	0.398	0.440	0.502	0.444	0.410	0.000	0.000	0.000	0.000
6	7	0.000	0.000	0.586	0.733	0.917	0.996	0.854	0.762	1.139	0.448	0.000	0.000
7	8	0.000	0.452	0.862	1.197	1.516	1.566	1.520	1.290	0.913	0.586	0.389	0.293
8	9	0.498	0.892	1.390	1.796	2.089	2.114	2.052	1.851	1.453	1.030	0.682	0.829
9	10	0.938	1.331	1.859	2.299	2.621	2.562	2.537	2.299	1.985	1.486	1.080	1.047
10	11	1.340	1.712	2.206	2.625	2.960	2.872	2.876	2.613	2.282	1.813	1.415	1.369
11	12	1.503	1.909	2.366	2.780	3.140	3.128	3.086	2.759	2.433	1.976	1.545	1.344
12	13	1.390	1.897	2.395	2.801	3.107	3.148	3.040	2.759	2.395	1.959	1.541	1.285
13	14	1.344	1.746	2.165	2.587	2.960	2.952	2.914	2.608	2.160	1.792	1.357	1.114
14	15	0.925	1.310	1.817	2.269	2.554	2.625	2.562	2.290	1.846	1.398	0.992	0.821
15	16	0.507	0.846	1.302	1.758	2.131	2.240	2.144	1.905	1.352	0.913	0.578	0.348
16	17	0.167	0.373	0.754	1.214	1.553	1.637	1.562	1.256	0.795	0.452	0.205	0.318
17	18	0.000	0.000	0.440	0.649	0.946	1.047	0.959	0.670	0.385	0.243	0.000	0.000
18	19	0.000	0.000	0.000	0.134	0.377	0.523	0.440	0.209	0.000	0.000	0.000	0.000
19	20	0.000	0.000	0.000	0.000	0.126	0.268	0.255	0.000	0.000	0.000	0.000	0.000

Table B2. Average hourly values of the a constant during the day in the months of the year. The values were determined from the measured global radiation and sunshine duration time series in Novi Sad in the period 1966–1970.

Start hour	End hour	J	F	M	A	M	J	J	A	S	O	N	D
4	5	0.00	0.00	0.00	0.00	0.07	0.37	0.12	0.00	0.00	0.00	0.00	0.00
5	6	0.00	0.00	0.00	0.22	0.39	0.47	0.47	0.35	0.00	0.00	0.00	0.00
6	7	0.00	0.00	0.32	0.46	0.36	0.39	0.59	0.45	0.17	0.11	0.00	0.00
7	8	0.00	0.35	0.38	0.39	0.36	0.36	0.34	0.38	0.43	0.35	0.18	0.04
8	9	0.39	0.39	0.38	0.34	0.37	0.34	0.35	0.37	0.44	0.36	0.29	0.17
9	10	0.42	0.42	0.39	0.35	0.35	0.32	0.31	0.40	0.42	0.39	0.31	0.28
10	11	0.43	0.39	0.40	0.35	0.32	0.34	0.34	0.37	0.40	0.38	0.30	0.30
11	12	0.42	0.40	0.35	0.34	0.31	0.35	0.35	0.38	0.38	0.41	0.30	0.35
12	13	0.47	0.41	0.35	0.34	0.32	0.37	0.34	0.37	0.35	0.41	0.31	0.37
13	14	0.39	0.39	0.35	0.33	0.31	0.34	0.29	0.33	0.39	0.38	0.30	0.35
14	15	0.41	0.37	0.32	0.34	0.33	0.37	0.31	0.45	0.43	0.35	0.32	0.30
15	16	0.38	0.36	0.32	0.30	0.33	0.32	0.28	0.31	0.40	0.38	0.29	0.35
16	17	0.25	0.33	0.31	0.37	0.30	0.35	0.34	0.37	0.44	0.38	0.22	0.05
17	18	0.00	0.00	0.18	0.37	0.38	0.34	0.43	0.33	0.34	0.10	0.00	0.00
18	19	0.00	0.00	0.00	0.45	0.39	0.42	0.40	0.38	0.00	0.00	0.00	0.00
19	20	0.00	0.00	0.00	0.00	0.15	0.22	0.17	0.00	0.00	0.00	0.00	0.00

where e_a is partial water vapor pressure in air (in Brunt's formula in [hPa], while in Konzelmann et al.'s formula in [Pa]) and T_a is air temperature at a height of 2 m in [K]. ε_a is parameterised according to Konzelmann et al. (1994) as

$$\varepsilon_a = \varepsilon_{cs} \times \left(1 - N^{1.6}\right) + 0.9552 \times N^{1.6}. \quad (A11)$$

Parameterization of r_{Hr}

As mentioned, r_{Hr} is a combined resistance for expressing the thermal radiative and convective heat exchanges,

$$\frac{1}{r_{Hr}} = \frac{1}{r_{Ha}} + \frac{1}{r_R} \; with \; r_{Ha}\left[sm^{-1}\right] = 7.4 \times 41 \times \sqrt{\frac{D}{U_{1.5}}}, \frac{1}{r_R} = \frac{4\varepsilon_{cl}\sigma T_a^3}{\rho c_p}, \quad (A12)$$

where D [m] is the diameter of the cylindrical body with which the human body is approximated (Campbell and Norman, 1998), $U_{1.5}$ is the wind speed at 1.5 m (around chest height). $U_{1.5}$ is calculated from U_{10} (wind speed at 10 m height) using a logarithmic wind profile approach. In this model, the direction of the walking human compared to the direction of wind speed is not taken into account.

Parameterization of M

According to Weyand et al. (2010) M for a walking human can be expressed as follows:

$$M = M_b + M_w, \quad (A13)$$

where M_b is the basal metabolic rate [W] (resting human), and M_w is the metabolic rate [W] referring to walking. Both terms can be parameterised knowing the most important human body features: sex, age [year], body mass, M_{bo} [kg] and body length, L_{bo} [cm]. According to Frankenfield et al. (2005) Mifflin et al.'s (1990) M_b parameterisation is one of the best,

$$M_b^{male}\left[kcal\ day^{-1}\right] = 9.99 \times M_{bo} + 6.25 \times L_{bo} - 4.92 \times age + 5, \quad (A14)$$

$$M_b^{female}\left[kcal\ day^{-1}\right] = 9.99 \times M_{bo} + 6.25 \times L_{bo} - 4.92 \times age - 161. \quad (A15)$$

To be able to obtain M_b in [Wm^{-2}], the surface of the human body A [m^2] has also to be estimated. Dubois and Dubois (1915) parameterisation is used taking M_{bo} and L_{bo} as inputs,

$$A = 0.2 \times M_{bo}^{0.425} \times \left(\frac{L_{bo}}{100}\right)^{0.725} \quad (A16)$$

M_w is parameterised according to Weyand et al. (2010) as follows,

$$M_w = 1.1 \times \frac{3.80 \times M_{bo} \times \left(\frac{L_{bo}}{100}\right)^{-0.95}}{A}. \qquad (A17)$$

Formula (1) in Weyand et al. (2010) refers to a walking distance of 1 m. Since the reference walking speed in our model is 1.1 m s^{-1}, Weyand et al.'s (2010) formula (1) is multiplied by a factor of 1.1. Dividing this by A, we will get M_w in [W m^{-2}].

Parameterization of λE_{sd}, λE_r, H_r, and W

λE_{sd}, λE_r, and H_r are parametrized according to Fanger (1970):

$$\lambda E_{sd} = 3.05 \times 10^{-3} \times \left(256 \times T_S - 3373 - e_a\right), \qquad (A18)$$

$$\lambda E_r = 1.7 \times 10^{-5} \times M \times \left(5867 - e_a\right), \qquad (A19)$$

$$H_r = 0.0014 \times M \times \left(34 - T_a\right). \qquad (A20)$$

where T_a is air temperature (°C) and e_a is actual vapour pressure [Pa].

W depends upon M. According to Auliciems and Kalma (1979) W is expressed as

$$W = 0.25 \times \left(M - M_b\right). \qquad (A21)$$

APPENDIX C.

Body mass index

The body mass index BMI is defined as follows:

$$BMI = \frac{M_{bo}}{\left(\frac{L_{bo}}{100}\right)^2} \qquad (A22)$$

It can be seen that it is easily calculated, which is why it is widely used to characterize the variability of the human body.